



The geochemical and temporal evolution of the continental lithosphere and its relationship to continental-scale faulting: The Karakoram Fault, eastern Karakoram, NW Himalayas

Richard J. Phillips

Institute of Geophysics and Tectonics, School of Earth and Environment, University of Leeds, Leeds, LS2 9JT, UK (R.J.Phillips@leeds.ac.uk)

Michael P. Searle

Department of Earth Sciences, University of Oxford, South Parks Road, Oxford, UK

Randall R. Parrish

NERC Isotope Geoscience Laboratory, British Geological Survey, Keyworth, Nottingham, UK

Department of Geology, University of Leicester, Leicester, UK

[1] New laser ablation multicollector–inductively coupled plasma–mass spectrometry and isotope dilution–thermal ionization mass spectrometry U–Pb ages, coupled with Sm–Nd isotope and geochemical analysis, define the temporal and geochemical evolution of the continental lithosphere in the eastern Karakoram, India, NW Himalaya. Our analysis demonstrates that magmatism occurred between ~108 and 69 Ma and ~22 and 13 Ma. The new age data, coupled with geochemical examination of the granitoids, confirm a parallel evolution with the western Karakoram in Pakistan and supports a model of regional continental crustal thickening and related metamorphism. Middle to Late Cretaceous magmatism immediately adjacent to the Karakoram fault suggests that crustal melting and associated metamorphism are unrelated to shearing along the fault. Miocene leucogranite magmatism occurred almost exactly concomitant with the emplacement of the Baltoro batholith in Pakistan. These trans-Karakoram leucogranites also display similar geochemical evolution trends. Our new data clearly link the leucogranites along the fault to the regional Baltoro batholith and related metamorphic complexes to the west. This supports previous work suggesting that magmatism and metamorphism were not syn-kinematic with continental-scale faulting. The data demonstrate that the Karakoram fault could not have accommodated lateral offset in this region prior to ~16 Ma, limiting the long-term averaged slip rate to a maximum of ~10 mm/yr.

Components: 12,000 words, 9 figures.

Keywords: Tibet; Karakoram; strike-slip fault; magmatism; U–Pb geochronology; geochemistry.

Index Terms: 8111 Tectonophysics: Continental tectonics: strike-slip and transform; 1115 Geochronology: Radioisotope geochronology; 1020 Geochemistry: Composition of the continental crust

Received 22 June 2012; **Revised** 20 December 2012; **Accepted** 27 December 2012; **Published** 19 March 2013.

Phillips, R. J., M. P. Searle, and R. R. Parrish (2013), The geochemical and temporal evolution of the continental lithosphere and its relationship to continental-scale faulting: The Karakoram Fault, eastern Karakoram, NW Himalayas, *Geochem. Geophys. Geosyst.*, 14, 583–603, doi:10.1002/ggge.20061.

1. Introduction

[2] Within orogenic belts, the spatial association of prominent shear zones with magmatic and metamorphic units has led many to infer a genetic relationship between faulting, melting, and changes in the thermal regime [e.g., Hollister and Crawford, 1986; Petford and Atherton, 1992; Tommasi *et al.*, 1994; Vauchez *et al.*, 1997]. This has led to the development of models that explain such relationships in terms of, e.g., shear heating, magma-assisted strain localization or fault-controlled magma emplacement. Despite the maturity of the discussion, limited progress has been made in resolving observed discrepancies between models and field data in some localities and this in turn has limited our understanding of orogenic processes with regard to the evolution of major transcurrent shear zones and their control (if any) on melting and metamorphism. Here we discuss one such example in the NW Himalaya, namely the 800 km long dextral Karakoram Fault and the magmatic and metamorphic units of the eastern Karakoram.

[3] Considerable discussion has concerned the origin and evolution of the magmatic and metamorphic rocks of the eastern Karakoram, NW Himalayas, and their relationship to the Karakoram Fault. One model (A) suggests that metamorphic rocks and leucogranites exhumed along the Karakoram Fault zone are syn-kinematic with regard to strike-slip shearing. This model interprets the fault as a crustal or lithospheric-scale fault and all granite ages provide a minimum age of ductile right-lateral shearing [Lacassin *et al.*, 2004; Valli *et al.*, 2007, 2008; Weinberg and Mark, 2008; Weinberg *et al.*, 2009]. The second model (B) suggests that metamorphism and most leucogranites exhumed along the fault were prekinematic with respect to strike-slip shearing, and that ages of granites along the fault will provide maximum ages of fault initiation and constrain the initiation of ductile deformation at the exposed structural level [Searle *et al.*, 1998; Phillips *et al.*, 2004; Phillips and Searle, 2007; Searle and Phillips, 2007; Wang *et al.*, 2009, 2012].

[4] Although the eastern Karakoram has previously been correlated with that of the southern Karakoram terrane in Pakistan [e.g., Searle, 1991; Searle *et al.*, 1998; Phillips *et al.*, 2004; Searle *et al.*, 2011], terrane association has formerly relied upon qualitative descriptors such as field observations, thin-section analyses, and mineral comparators for specific rock types. At present no detailed quantitative study has been undertaken to examine the regional heterogeneity in geochemical, isotopic, and geochronological

data both along- and across-strike of the Karakoram Fault, specifically between the eastern and western Karakoram. Such a study is now pertinent because recent discussion [e.g., Leech, 2008; Searle and Phillips, 2009; Parrish, 2009] has linked the initiation and development of the Karakoram Fault to the evolving continental lithosphere now represented by the eastern Karakoram.

[5] In this paper, we couple laser ablation multicollector-inductively coupled plasma-mass spectrometry (LA-MC-ICP-MS) and isotope dilution-thermal ionization mass spectrometry (ID-TIMS) U-Pb geochronology with analysis of Sm-Nd isotopes and major and trace elements via modeling of large-ion lithophile element (LILE) evolution, magmatic fractionation trends, isotopic mixing models, and evolution trends. We show that the chronology of metamorphism and magmatism of units that bound the Karakoram Fault in the eastern Karakoram of India match very closely with that of the undeformed Baltoro Karakoram, several hundred kilometers away in Pakistan. For the eastern Karakoram, we suggest that metamorphism and magmatism was not a result of shear heating in relation to faulting. Instead, the new geochemical and U-Pb geochronological data set relate granite petrogenesis and metamorphism to the regional Baltoro batholith and related metamorphic complexes to the west. The magmatic and metamorphic units of the eastern Karakoram are therefore considered part of a sequence that is formed in response to regional crustal thickening and melting, rather than related to local dextral faulting since the Miocene. These data sets limit on the age and offset of the Karakoram Fault and thus its role in continental tectonics during the Himalaya-Tibet Orogeny.

2. Geology of the Eastern Karakoram, Ladakh

[6] The eastern Karakoram in the Nubra-Siachen and Pangong ranges of northern Ladakh are the eastward continuation of the Baltoro-Hunza central Karakoram and the Hindu Raj-Hindu Kush region of Pakistan and are geologically equivalent to the Qiangtang terrane of central Tibet. The Shyok suture zone to the south separates the Karakoram-Qiangtang terrane from the Kohistan arc-Ladakh-Gangdese granite batholith of southern Lhasa block. These terranes are all located along the Asian plate north of the Indus Yarlung Tsangpo suture zone, the site of the India-Asia collision, which closed at ~50 Ma [e.g., Rowley, 1996; Najman *et al.*, 2010].

Following the Early Eocene collision between India, the Kohistan arc, and the thickened crust of Eurasia, regional metamorphism spread both across the Indian plate to the south along the Himalaya, and across the Karakoram terrane to the north. Migmatization and crustal melting led to intrusion of leucogranites along the Greater Himalaya between ~24 and 15 Ma and intrusion of the Baltoro granite batholith between ~22 and 17 Ma [Searle *et al.*, 2010].

[7] With regard to regional nomenclature, the common spelling “Karakoram” is adopted here, as opposed to the alternative “Karakorum” used in recent publications. “Karakoram” derives from the old Turki script and translates as “black gravel” or “black ground” and likely refers to the prominent Permo-Carboniferous black slates and shales of the Aghill-Shaksgam area and the Northern Karakoram Terrane. In 1877 the official spelling “Karakoram” was used in the first survey map of the region and appears in subsequent editions of official survey maps of India and Pakistan. The adopted nomenclature is defined and robustly defended by *Burrard* [1929].

[8] The eastern Karakoram contains regional amphibolite and greenschist facies metamorphic rocks, migmatites, precollision calc-alkaline diorites, granodiorites and stromatic migmatites, and postcollision two-mica ± garnet leucogranites. These rocks are separated from the Baltoro Karakoram by the right-lateral strike-slip Karakoram Fault. In the Pangong-Nubra region the fault splays into two prominent branches, the Pangong Fault to the NE and the Tangtse Fault to the SW. In between the two faults the Pangong Range comprises transpressionally uplifted high-grade metamorphic rocks, migmatites, and granites.

[9] The geology of the eastern Karakoram is dominated by a suite of precollisional hornblende-biotite diorites, orthogneisses, and granites that intrude the Eurasian Plate Paleozoic-Mesozoic sediments, and a series of postcollisional leucogranite intrusions that include major dyke-sill networks and minor plutons. These eastern Karakoram granitoids (EKG) extend along the Nubra-Siachen valley and throughout the Pangong Transpressional Zone (PTZ), which is bounded by the major right-lateral Karakoram Fault (Figures 1 and 2). Following *Phillips et al.* [2004], *Phillips and Searle* [2007], and *Phillips* [2008] the Nubra-Siachen and PTZ granitoids are subdivided, on the basis of lithology, into two magmatic units. The Nubra-Siachen leucogranites comprise a sheeted complex of postcollisional K-feldspar megacrystic muscovite-biotite leucogranite and biotite leucogranite with garnet-biotite–muscovite leucogranite dykes

and orbicular and porphyritic microgranite. The Arganglas hornblende-biotite diorites bound the leucogranites to the northeast.

[10] The PTZ granitoids comprise (1) Tangtse-Darbuk leucogranites (postcollisional biotite leucogranite dykes and garnet-muscovite-biotite leucogranite, Kfs-megacrystic muscovite-biotite leucogranite, and biotite leucogranite sheets), (2) Muglib Migmatite Complex (biotite granite leucosomes and hornblende-biotite melanosomes that outcrop in the Tangtse valley adjacent to the Pangong strand of the Karakoram Fault), and (3) Pangong orthogneiss (hornblende-biotite diorites that form the dominant basement of the PTZ).

[11] Below, we provide a detailed description of all magmatic units of the eastern Karakoram and define specific quantitative comparators in order to explore the scale of geochemical and temporal variation and their possible relation to regional faulting. Quantitative comparators include: (1) major and trace element analyses, (2) LILE modeling, (3) analysis of fractionation trends, (4) isotopic mixing models, (5) isotopic evolution trends, and (6) coupled ID-TIMS and LA-MC-ICP-MS U-Pb age dating of magmatic events. Although use of a single comparator alone can only provide tentative details of chemical variation and terrane correlation, the combined analyses provide sufficient evidence for closely matched comagmatic petrogenetic histories.

3. Geochemistry of Eastern Karakoram Granitoids

[12] In order to provide an understanding of the evolution of magmatism across the Karakoram and to explore any potential link to the initiation of the Karakoram Fault, 17 samples of magmatic rocks from the Nubra-Siachen region and the Pangong Transpressional Zone were analyzed for their geochemical and isotopic characteristics. These samples were grouped on the basis of a comagmatic association determined by their field relationships, age, and petrology [*Phillips et al.*, 2004; *Phillips and Searle*, 2007; *Phillips*, 2008]. The sample data are modeled on the basis of the crystallization age for each comagmatic group as defined by coupled LA-MC-ICP-MS and ID-TIMS U-Pb data outlined in section 4 (see also, Figures 3–5). The comagmatic groups are:

- (A) A precollisional middle Cretaceous diorite suite. This suite includes the Arganglas diorite (P142), the Muglib Migmatite Complex restite (P112) and the Pangong orthogneiss (P129).

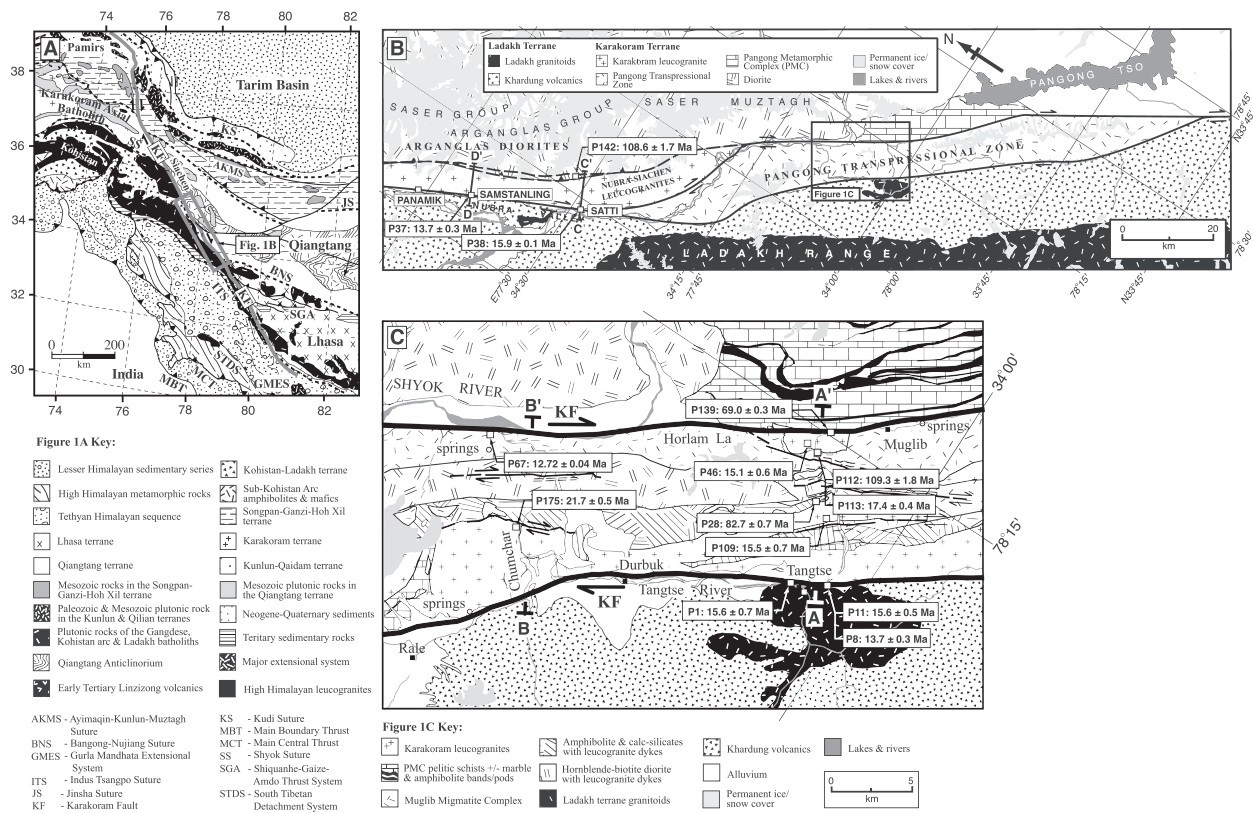


Figure 1. Location and simplified geology of the eastern Karakoram, Ladakh, NW India. (A) Regional geological map of the NW Himalaya and western Tibet. Inset box shows the location of the eastern Karakoram. Further detail can be obtained in, e.g., Searle [1992], Yin and Harrison [2000], Schwab et al. [2004], and Robinson et al. [2012]. (B) Geology of the eastern Karakoram. (C) Detail of the geology of the Pangong Transpressional Zone (PTZ). Figures 1B and 1C display the sample locations and U-Pb ages for all granitoids analyzed. See Figure 2 for cross-sections. Modified from Phillips et al. [2004], Phillips and Searle [2007], and Phillips [2008].

- (B) A precollisional Late Cretaceous granitoid suite (within the Pangong Transpressional Zone). This suite includes precollisional granitoid host rocks (P28, P101, P103, P139, P172, P184).
- (C) A postcollisional Miocene leucogranite suite. This includes the Nubra-Siachen leucogranites (P35, P38, P72a), the Tangtse-Darbuk leucogranites (P1, P5, P46, P175) and the Muglib Migmatite Complex leucosome (P113).

[13] Table S1 presents a summary of the major and trace element data for representative phases of the eastern Karakoram granitoids and includes their formation and member names as well as their locations. Figures 1 and 2 show the sample sites for geochemical analysis, while Figures 7 and S1–S4 in the auxiliary material display the data.¹

[14] The results of the Rb-Sr and Sm-Nd isotopic analysis are displayed in Table S2 and Figures 6 and 7. The isotope data reported in Table S2 give

¹All Supporting Information may be found in the online version of this article.

¹⁴³Nd/¹⁴⁴Nd and ⁸⁷Sr/⁸⁶Sr calculated both for the time of crystallization (which is used to characterize magma compositions for the different intrusive episodes dated) and for 15 Ma (which is appropriate when considering possible local crustal sources for the Miocene leucogranites). Details for all analytical procedures are presented in the auxiliary material.

3.1. Precollisional Magmatism

3.1.1. Middle Cretaceous Diorites

[15] The metaluminous middle Cretaceous diorites define a calc-alkaline trend with little variation in element abundance between samples. The suite displays major- and trace-element trends similar to the Late Cretaceous granitoids, although the latter are more enriched in LILE. The diorites have low Ti ($TiO_2 < 0.8\%$), moderate LILE (average Rb = 86 ppm, Sr = 252 ppm, Ba = 256 ppm), depleted high field strength elements (HFSE) with a high Rb/Sr ratio (average = 0.34), and moderate Th/U (average = 3.0).

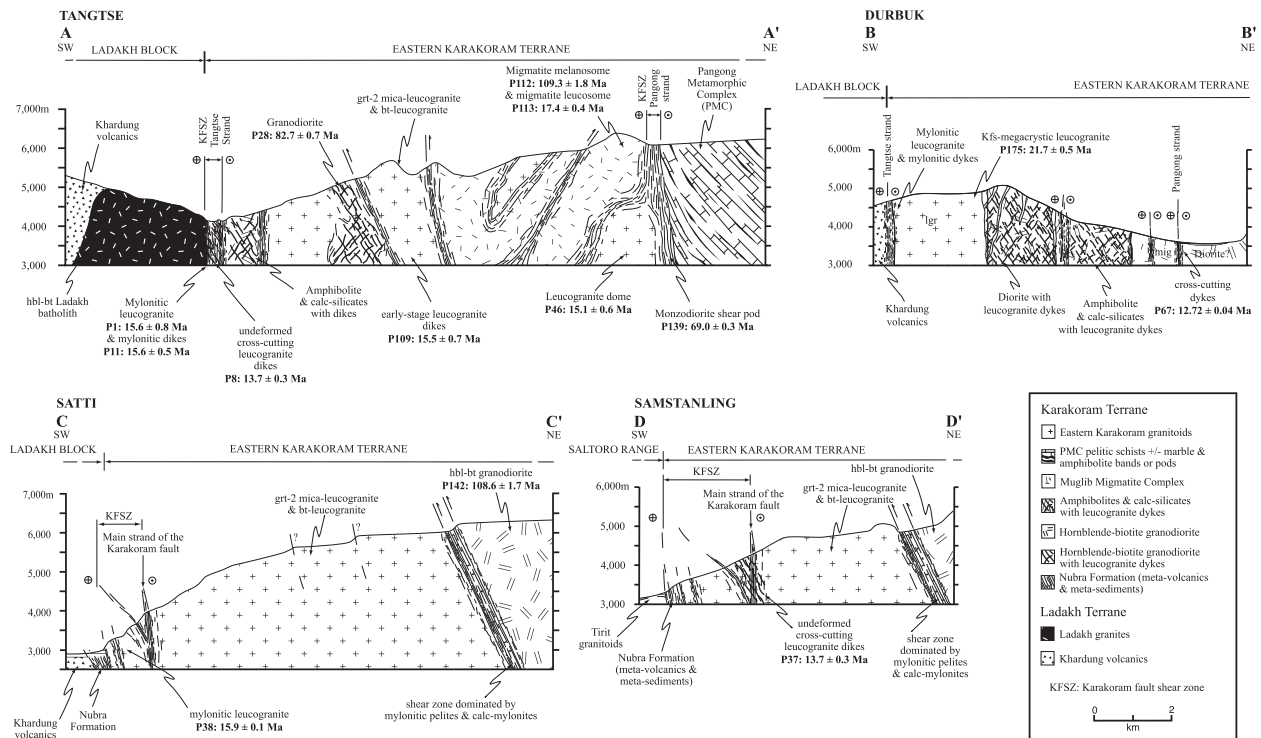


Figure 2. Cross-sections through the eastern Karakoram terrane showing the structural relations between units and the U-Pb ages (see Figure 1 for locations). Modified from Phillips *et al.* [2004], Phillips and Searle [2007], and Phillips [2008].

The group shows moderate LILE/HFSE ratios with negative anomalies in Nb and Sr. Because the sample size is small, it is not possible to define a source trend. The suite displays initial $^{87}\text{Sr}/^{86}\text{Sr}$ in the range 0.710317–0.714870 with low $^{143}\text{Nd}/^{144}\text{Nd}$ ratios corresponding to ϵNd values between -7.5 and -8.9 (Table S2).

[16] This group plots within the field of the equivalent-aged hbl-bt granitoids of the Karakoram terrane (e.g., K2 – Broad Peak gneiss; Figures 7 and 8). The Nd model ages of the diorites range from 1.46 to 1.56 Ga, an age range compatible with an inherited Precambrian component within zircons from K2 [Crawford and Searle, 1992].

3.1.2. Late Cretaceous Granitoids

[17] This suite displays a wide variation in SiO_2 content (63–77 wt %) and plots within the monzodiorite and syenogranite field of an R_1R_2 diagram (Figures S1–S4). Assuming a comagmatic relationship, this variation may indicate a magmatic fractionation trend. The group traverses fields IV–II in the AB diagram, becoming increasingly leucocratic and crossing the metaluminous-peraluminous domain. The group is subalkalic with moderate variation in total alkali content. Some fractionation between samples is evident from element abundance variation

with increasing SiO_2 and depletion in Sr, P, Zr, and Ti, reflecting a reduction in plagioclase, ferromagnesian oxides and zircon (Table S1).

[18] The suite displays low Ti ($\text{TiO}_2 < 0.8\%$), enriched LILE (average Rb = 100 ppm, Sr = 412 ppm, Ba = 412 ppm), relative depletion in HFSE with low Rb/Sr ratio (average = 0.24), moderate Th/U (average = 4.5), and modest variation in light rare earth element/heavy rare earth element (LREE/HREE) ratios (Table S1A; $[\text{La}/\text{Yb}]_N$ and Eu/Eu^*). The relative depletion of HREE with respect to LREE, coupled with a slight enrichment in HREE between Er and Lu, may reflect the presence of amphibole in the source. The suite exhibits low initial $^{87}\text{Sr}/^{86}\text{Sr}$ (0.704816–0.709269) and highly radiogenic $^{143}\text{Nd}/^{144}\text{Nd}$ ratios, corresponding to ϵNd values between +1.5 and +3.0 (Table S2). These ratios are comparable to the 40 Ma hbl-bt granite from the Hushe plutonic unit in the Karakoram ($^{87}\text{Sr}/^{86}\text{Sr} = 0.705988$, $\epsilon\text{Nd} = 0.2$; Searle *et al.* [2010]), although the Hushe samples have lower ϵNd values.

3.2. Postcollisional Magmatism

3.2.1. Miocene Leucogranites

[19] The postcollisional EKG suite ranges in SiO_2 content between 67 and 75 wt % and defines a narrow



Figure 3. Field localities within the eastern Karakoram. (A) Cross-section through the PTZ, along the Tangtse valley. Strands of the Karakoram Fault bound the PTZ. The sample locations for P1, P8, P11, P28, P46, P109, P112, P113, and P139. LTV – Ladakh terrain volcanics; LTG – Ladakh terrain granites; AMP – amphibolite; D – diorite; TDL – Tangtse-Darbuk leucogranites; MIG – Muglib Migmatite Complex; PMC – Pangong Metamorphic Complex. (B) Samples P37 and P38 from the Nubra-Siachen leucogranites, Nubra valley. (C) Sample P142 from the Arganglas diorites, NE of the Nubra-Siachen leucogranites. (D) Leucogranite dyking within amphibolite, Tangtse Valley. Sample P109 represents the oldest dyke set. (E) Overview of the Muglib dome (sample P46) and the Muglib Migmatite Complex (samples P112 and P113). The Pangong strand of the Karakoram Fault bounds the dome to the ENE. (F) Close-up of part of the Muglib Migmatite Complex, showing sample localities for P112 and P113. (G) Fault-parallel leucogranite dyking within the Shyok Valley. The dykes traverse the Pangong Transpressional Zone and are observed to crop out within the Tangtse Valley. (H) Leucogranite sheet (sample P175) within the Shyok Valley.

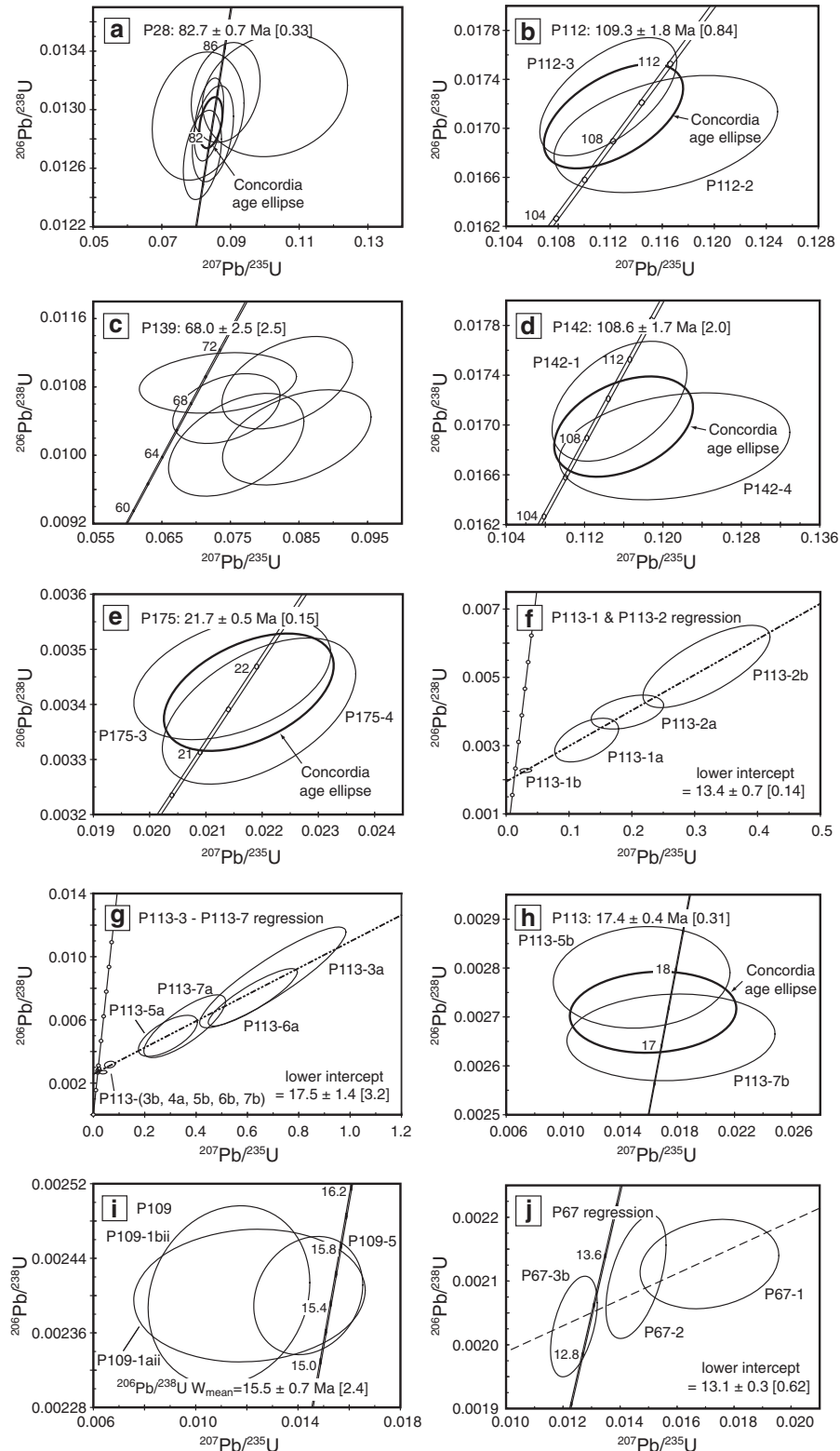


Figure 5. (a–j) LA-MC-ICP-MS Concordia plots for samples analyzed in addition to ID-TIMS (see section 4 and Tables S6 and S7). Data point error ellipses are 2σ .

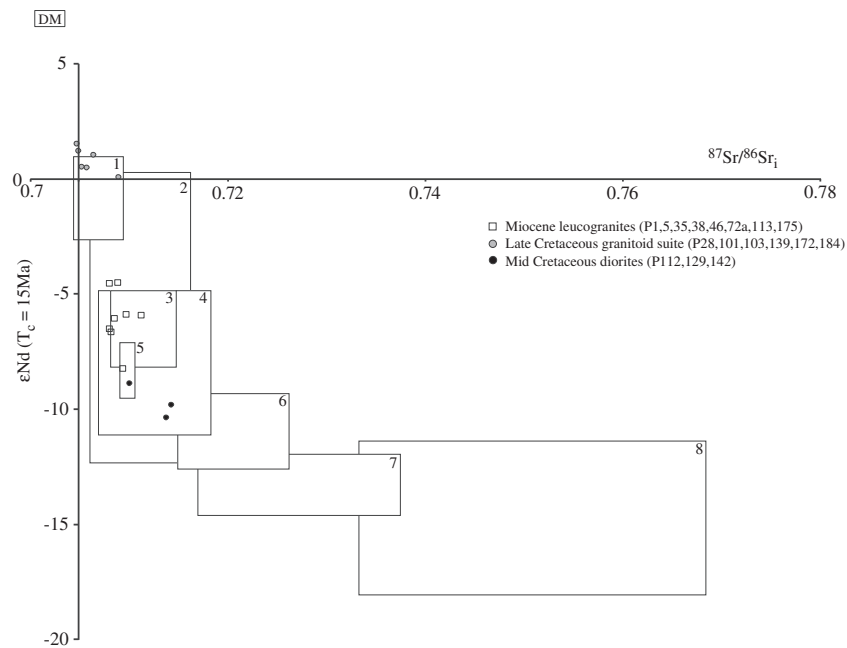


Figure 6. ϵNd vs. $^{87}\text{Sr}/^{86}\text{Sr}_i$ for the eastern Karakoram granitoids. The data are plotted with reference to typical Karakoram-Tibet-Himalaya values: (1) Trans-Himalayan batholith [Miller *et al.*, 1999; Allègre and Othman, 1980], (2) Karakoram precollisional hbl-bt granitoids [Crawford and Searle, 1992; Thow, 2004], (3) Baltoro leucogranites [Crawford and Windley, 1990; Thow, 2004; Maheo *et al.*, 2009], (4) Karakoram leucogranites [Schärer *et al.*, 1990; Crawford and Windley, 1990; Thow, 2004], (5) Tibetan calc-alkaline volcanics [Miller *et al.*, 1999], (6) Karakoram lamprophyres [Thow, 2004], (7) Tibetan potassic and ultrapotassic volcanics [Miller *et al.*, 1999], (8) high Himalayan leucogranites [Allègre and Othman, 1980; Vidal *et al.*, 1982, 1984; Deniel *et al.*, 1987; Inger and Harris, 1993; Searle *et al.*, 1997]. All initial ratios are recalculated to 15 Ma and $^{143}\text{Nd}/^{144}\text{Nd}$ ratios are normalized to $^{146}\text{Nd}/^{144}\text{Nd}=0.7219$. DM represents N-MORB averaged from Saunders *et al.* [1988].

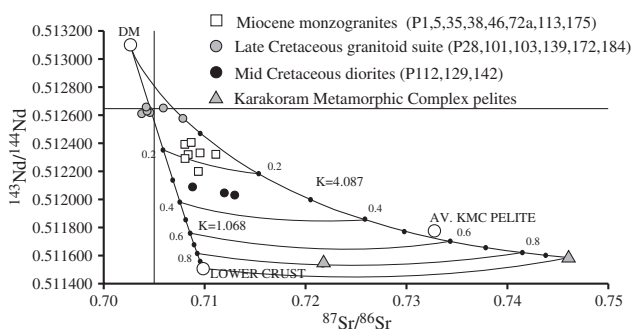


Figure 7. $^{143}\text{Nd}/^{144}\text{Nd}$ vs. $^{87}\text{Sr}/^{86}\text{Sr}$ initial ratios and two-component mixing lines for the eastern Karakoram granitoids. KMC pelites taken from this study and Thow [2004]. The DM field has $^{87}\text{Sr}/^{86}\text{Sr}=0.70278$, $^{143}\text{Nd}/^{144}\text{Nd}=0.513094$, Sr = 90 ppm, Nd = 7.3 ppm. The lower crust field has $^{87}\text{Sr}/^{86}\text{Sr}=0.71000$, $^{143}\text{Nd}/^{144}\text{Nd}=0.511500$, Sr = 300 ppm, Nd = 26 ppm. Both DM and lower crust taken from Miller *et al.* [1999]. The shape of the mixing hyperbolae are characterized by the parameter $K=(\text{Nd}/\text{Sr})_A/(\text{Nd}/\text{Sr})_B$, where A and B represent the two end-member mixing components. Points on the hyperbolae indicate the weight fraction of the lower crust or pelite relative to DM.

subalkalic, with a narrow range in total alkali (Na + K) content. These elemental variations are displayed in Figure S1B, the group plotting as a small array in the peraluminous and leucocratic domain.

[20] The suite exhibits low Ti ($\text{TiO}_2 < 0.6\%$), enriched LILE (average Rb = 164 ppm, Sr = 637 ppm, Ba = 1165 ppm), depleted HFSE with elevated Rb/Sr (average = 0.26), and a high Th/U ratio (average = 6.08). The high LILE/HFSE ratio, coupled with a large negative Nb anomaly, indicates that the leucogranite suite is rather depleted. Such a signature may relate to remelting of crustal lithologies with a preexisting mantle component [e.g., Tarney and Jones, 1994], the presence of local adakites with a more transitional I-S type isotope chemistry derived by mantle melting or, more likely, may relate to partial melting of grt-bearing eclogite or amphibolite-bearing rocks in the lower crust [Mahéo *et al.*, 2009].

[21] Trace element data for the leucogranites defines a lower-crustal or midcrustal origin and are geochemically similar to the Baltoro leucogranites of the Karakoram batholith of Pakistan. Given these

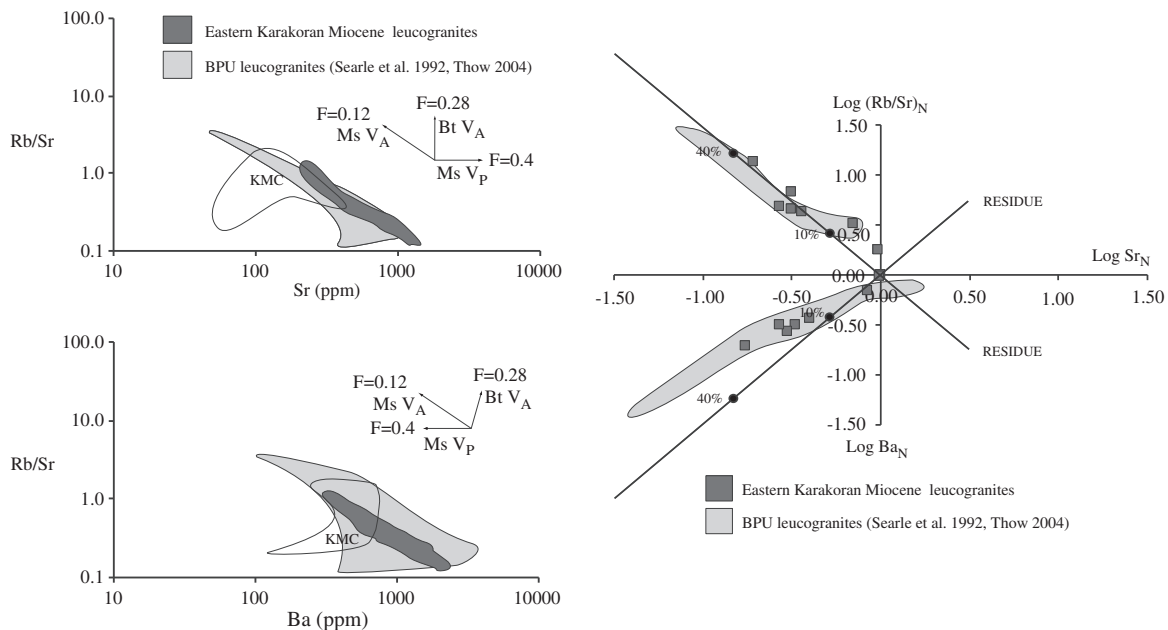


Figure 8. Comparative trace element modeling for the eastern Karakoram and the Baltoro leucogranites [after *Inger and Harris, 1993*]. (A) Rb/Sr vs. Sr diagrams. (B) Rb/Sr vs. Ba. The Karakoram Metamorphic Complex field (KMC) represents sampled pelites (this study and *Thow [2004]*). Melt vectors represent partial melting reactions for muscovite (Ms) or Biotite (Bt) vapor absent (V_A) or vapor present (V_P) reactions. LILE trends for the Miocene leucogranites of the eastern Karakoram (EK) compared to those of the Baltoro leucogranites. The EK and Baltoro samples were normalized to the least siliceous of the EK group (P113). Lines are Rayleigh fractionation trends showing percentage fractional crystallization for a typical Baltoro-type assemblage (65% plagioclase, 12% orthoclase, 18% biotite, 3% sphene, and 2% apatite).

apparent similarities, LILE modeling of the eastern Karakoram leucogranites was undertaken in order to examine if these regions do indeed share a similar petrogenetic history for the Miocene (see below). The postcollisional magmatic suite displays moderate initial $^{87}\text{Sr}/^{86}\text{Sr}$ (0.708238–0.711905) and low $^{143}\text{Nd}/^{144}\text{Nd}$ ratios corresponding to ϵNd values between -3.1 and -6.8 (Table S2). As illustrated in Figure 6, the data plot in the enriched quadrant of the Sr-Nd isotope diagram and overlap with the Sr-Nd fields for the Miocene leucogranites of the Baltoro region. The Nd model ages of the EKG leucogranites, relative to depleted mantle, range from 1.13 to 1.41 Ga, while similar leucogranites from the Baltoro range from 0.98 to 1.29 Ga [*Searle et al., 2010*].

[22] *Searle et al. [1992, 2010]* suggested that the Baltoro suite of the Pakistan Karakoram is sourced via dehydration melting of biotite-rich pelites of the Karakoram metamorphic complex (KMC). LILE modeling [*Harris and Inger, 1992; Inger and Harris, 1993; Harris et al., 1995*] offers a means to explore this suggestion and provides an opportunity to examine the comparative petrogenesis of the postcollisional leucogranites of the eastern Karakoram.

[23] *Harris and Inger [1992], Inger and Harris [1993], and Harris et al. [1995]* have demonstrated

that melting of pelitic rocks follows three possible reactions: (1) vapor-saturated melting of muscovite ($\text{Ms } V_P$), $\text{ms} + \text{pl} + \text{qtz} + \text{H}_2\text{O} = \text{Sil} + \text{melt}$, (2) vapor absent melting of muscovite ($\text{Ms } V_A$), $\text{ms} + \text{pl} + \text{qtz} = \text{Kfs} + \text{Sil} + \text{melt}$, or (3) vapor absent melting of biotite ($\text{Bt } V_A$), $\text{bt} + \text{Sil} + \text{qtz} + \text{pl} = \text{grt} \pm \text{Kfs} + \text{melt}$. The melt reactions for a typical pelite (10% biotite, 20% muscovite, 15% plagioclase, 15% garnet, and 35% quartz) were modeled by *Harris and Inger [1992]* using distribution coefficients between restite and melt phases for Rb, Sr, and Ba. The $\text{Ms } V_P$ reaction was enriched in Sr relative to that for $\text{Ms } V_A$ resulting in a comparatively lower Rb/Sr for $\text{Ms } V_P$. Figure 8A displays LILE data for EKG leucogranites and typical Baltoro granites plotted in Rb/Sr vs. Sr and Rb/Sr vs. Ba coordinate space. The inset diagram displays the melt vectors modeled by *Inger and Harris [1993]* for the melt reactions $\text{Ms } V_P$, $\text{Ms } V_A$ and $\text{Bt } V_A$. The diagram illustrates that the Miocene leucogranites of the EKG overlap with the Baltoro field and follow the same trend. While parallel to the $\text{Ms } V_A$ melt vector, the breadth of the Baltoro field may indicate an additional $\text{Bt } V_A$ melt reaction. In addition, neither the EKG leucogranite field nor the Baltoro field trend away from the KMC in the direction of either melt vector. Therefore, the source rock, while still

crustal, may not reflect the KMC assemblage currently exposed in the Karakoram.

[24] *Crawford* [1988] and *Crawford and Searle* [1992] have shown that comagmatic grt-bt-ms- and bt-ms-leucogranite suites of the Baltoro are related through fractionation. They suggested that trace element abundances within these suites could be replicated by fractionating the assemblage 65% plagioclase, 12% orthoclase, 18% biotite, 3% sphene, and 2% apatite. The EKG leucogranites are modeled using the same assemblage on a Log Rb/Sr vs. Log Sr vs. Log Ba tri-variate plot normalized to the least siliceous member of the group (Figure 8). Note that the extent of the Baltoro field for Log Sr_N vs. Log Ba_N indicates that these leucogranites display less siliceous end-members compared with those of the EKG. Figure 8 illustrates that the eastern Karakoram leucogranite suite closely tracks the fractionation trend of the Baltoro and demonstrates that they have evolved along a similar geochemical pathway.

[25] The leucogranites display low initial ⁸⁷Sr/⁸⁶Sr and elevated ¹⁴³Nd/¹⁴⁴Nd ratios when compared with similar crust-derived rocks from the High Himalaya; the converse being true for rocks of the precollisional, Andean-type, Trans-Himalayan Batholith. This latter relationship lends further credence to the idea that the EKG leucogranites evolved by crustal anatexis that may have included possible partial melting of amphibole-bearing rocks in the lower crust [*Mahéo et al.*, 2009].

[26] In summary, for both precollisional and postcollisional units, it is evident that although there is some local geochemical heterogeneity, the amplitude of isotopic and chemical variation between the Baltoro and the EKG is negligible, reflecting bulk geochemical homogeneity across the region. It is therefore considered that the two regions share a closely related petrogenetic history. Section 4 outlines the geochronology of the Karakoram and outlines the comagmatic relationships across the region.

4. U-Pb Geochronology

[27] We present the results of new LA-MC-ICP-MS and ID-TIMS U-Pb analysis of samples taken from the Nubra valley and the Pangong Transpressional Zone in the eastern Karakoram (Figures 1–5 and 9, Tables S3–S8). Samples that fully represent all of the observed mineralogical and structural variation within the terrane were selected. ID-TIMS methods were used with a small number of crystals

analyzed for each sample in order to provide an initial first-order characterization of terrane age variation. Additional LA-MC-ICP-MS data were collected to assist in resolving complexities and to supplement the ID-TIMS data set.

4.1. Precollisional Granitoids

4.1.1. Dioritic to Monzodioritic Precollisional Magmatism, Pangong Transpressional Zone

[28] Precollisional sheets and pods of hornblende-biotite orthogneiss are preserved along the northern boundary of the Nubra valley (Arganglas Range) and in the Pangong Transpressional Zone (Figures 1 and 2). These gneissic rocks are compositionally variable and include monzodiorite (P139) to tonalite-diorites (P28, P112, and P142), reflecting the full range of lower crustal protoliths exposed within the eastern Karakoram.

4.1.1.1. Sample P28, Diorite, Tangtse Valley

[29] Sample P28 has the assemblage pl + hbl + bt + Kfs + qtz ± cpx and represents a portion of Karakoram lower crustal country rock. The diorite forms a strongly foliated, linear intrusive belt, which extends parallel to the Pangong and Tangtse strands of the Karakoram fault. Throughout the Pangong Transpressional Zone the diorite is intruded by numerous postcollisional leucogranite dykes and, on its southern margin, is intruded by a kilometer-sized leucogranite sheet. Two zircon morphologies were identified for ID-TIMS. Fraction Z1 consists of inclusion-rich euhedral grains, 100 μm in length, whereas fraction Z2 comprises grains of similar shape and composition but are 200 μm in length. Additional LA-MC-ICP-MS data proved useful in complementing the ID-TIMS analyses.

[30] Isotope dilution-thermal ionization mass spectrometry analysis P28 Z2 is concordant with a ²⁰⁶Pb-²³⁸U age of 82.1 ± 0.8 Ma, while P28 Z1 is discordant with a ²⁰⁶Pb-²³⁸U age of 84.9 ± 1.4 Ma (Figure 4a and Table S3). Both fractions contain low amounts of uranium and an elevated Th/U ratio incompatible with other fractions from the middle to Late Cretaceous sample assemblage (e.g., P112 Z2; P139 Z1-Z3; P142 Z1, Z4-Z5). Six LA-MC-ICP-MS analyses on four separate grains were conducted for sample P28 (Figure 5a and Table S6) and provide an age of 82.7 ± 0.7 Ma (mean square weighted deviation (MSWD)=0.33), compatible with the concordant ID-TIMS analysis for P28 Z2.

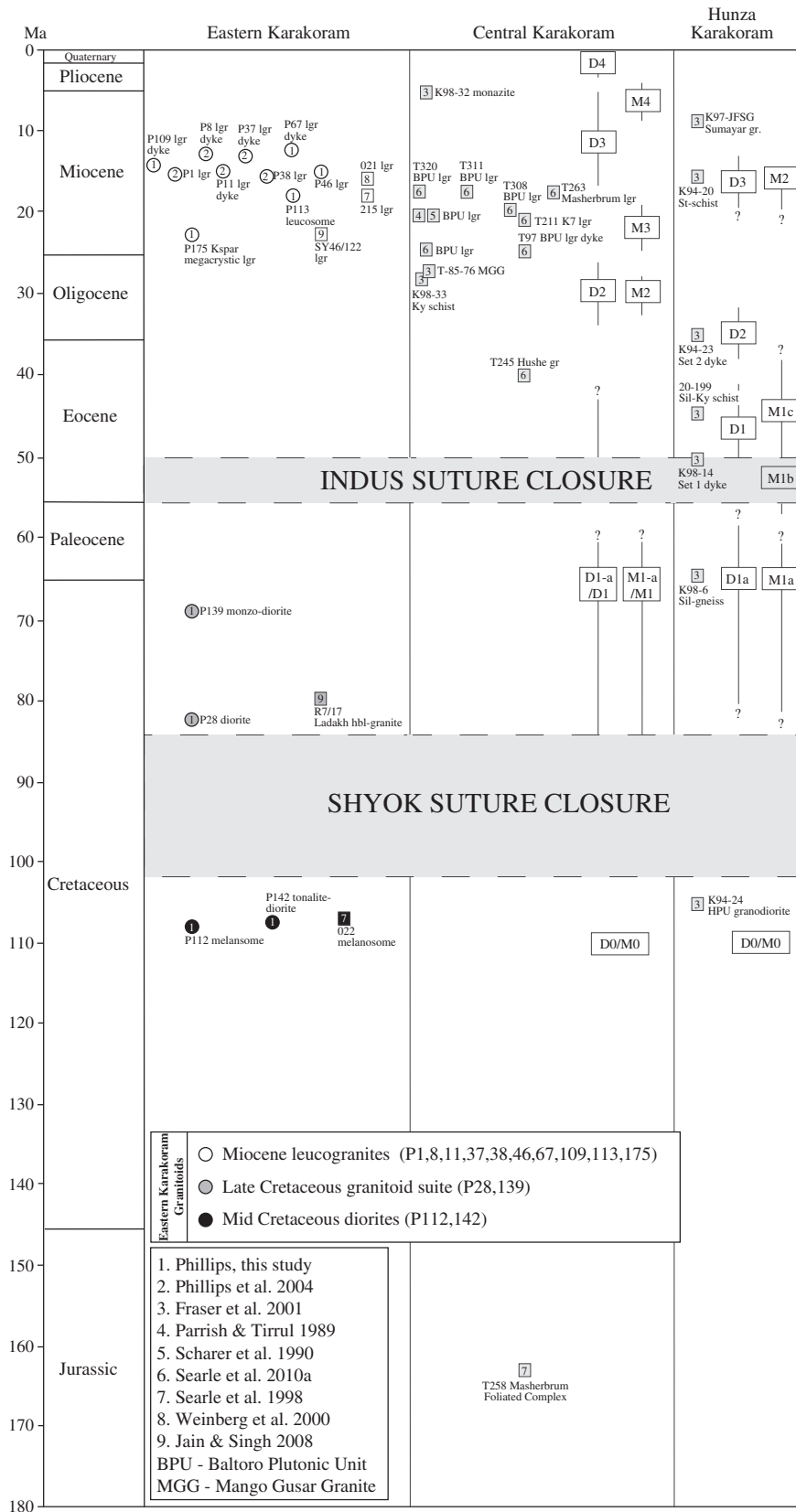


Figure 9. Summary chronology of magmatism, deformation and metamorphism in the Karakoram.

4.1.1.2. Sample P112, Diorite, Tangtse Valley

[31] This restitic melanosome, a lower crustal protolith from the Muglib Migmatite Complex, consists of the assemblage $pl + hbl + bt + Kfs + qtz \pm cpx$. The migmatite wraps around an intrusive leucogranite dome (sample P46) on the Pangong strand of the Karakoram Fault and displays a dominant foliation within the melanosome that parallels the restite-leucogranite boundary [Weinberg and Searle, 1998; Weinberg and Mark, 2008]. The leucosome (sample P113) is present as convolute ribbons, which coalesce to form meter-sized globules. U-Pb analysis of the migmatite complex provides constraints on both the age of lower crustal protoliths (sample P112) and the timing of in situ melting (sample P113).

[32] The migmatitic melanosome was dated using two analyses of zircons that differ in size and quality. Fraction P112 Z1 comprised zircons that were generally larger, contained more inclusions and were U-poor in comparison to P112 Z2 (Figure 5b and Table S3). In an attempt to improve the common lead correction for P112, a correction based upon the common lead in feldspars was used from the leucosome P113 on the assumption that the common lead composition in the melt was equivalent to that in the restite (Table S5). Although this improved the correction, a nontrivial 2σ error in the ^{207}Pb - ^{235}U age remained for both analyses.

[33] P112 Z1 and Z2 gave ^{206}Pb - ^{238}U ages of 107.9 ± 1.8 and 19.7 ± 0.5 Ma, respectively, suggesting that fraction Z2 was contaminated by leucosome-related zircons. The age of the restite is therefore best estimated by the ^{206}Pb - ^{238}U age of 107.9 ± 1.8 Ma from fraction Z1 and is within error of the SHRIMP age of 106.3 ± 2.3 Ma [Searle *et al.*, 1998]. Seven LA-MC-ICP-MS analyses on five separate grains provide a concordant age for the restitic melanosome and information regarding the age of the associated leucosome. Grains P112-2 and P112-3 yield a Concordia age of 109.3 ± 1.8 Ma (Figure 5b and Table S6), within error of the ID-TIMS measurement for P112 Z1. The improved accuracy and the multiple measurements favor the use of 109.3 ± 1.8 Ma as the best estimate of age for restitic zircons in sample P112.

[34] The younger ID-TIMS analysis, P112 Z2, is indicative of the age of in situ melting and is broadly compatible with age data for the leucosome sample P113. Five laser ablation analyses from grains P112-4 to P112-6 are discordant and provide a regression with a lower intercept of 12.0 ± 3.1 Ma (MSWD=1.03). Due to the high relative common Pb and low U, the error for the younger component cannot be resolved more precisely, and is not in

agreement with the ID-TIMS analyses for P112 Z2. Because older zircons are prevalent in this sample it may be that analysis P112 Z2 consisted of a mixture of ~ 12 Ma magmatic/metamorphic zircons with older magmatic restitic grains ~ 109 Ma old. The age of in situ melting is resolved through analysis of P113 (below).

4.1.1.3. Sample P139, Monzodiorite, Muglib

[35] This sheared gneissic pod within the Pangong fault zone consists of $pl + Kfs + hbl + bt + qtz \pm cpx$ and displays a preexisting deformation fabric that lies oblique to the main foliation within the shear zone. The pod is thought to represent predeformed wall-rock that bounded the shear zone and has subsequently been exhumed within the Pangong fault strand and offers further information on the precollisional lower crustal protolith within the eastern Karakoram.

[36] Isotope dilution-thermal ionization mass spectrometry fractions P139 Z1, Z2, and Z3 are each concordant within error, although they display variable ^{206}Pb - ^{238}U ages (Figure 4c and Table S3). Despite a negligible difference in U-content between fractions, P139 Z2 and Z3 display elevated $^{206}\text{Pb}/^{204}\text{Pb}$ ratios and lower Th/U ratios by comparison to fraction Z1. Therefore, given that Z1 appears to have suffered relative lead loss, the ^{206}Pb - ^{238}U Concordia age of 69.0 ± 0.3 Ma (MSWD=0.96) for fractions Z2 and Z3 reflects the sample age more precisely. By comparison, the mean weighted ^{207}Pb - ^{235}U age of the overlapping fractions Z1, Z2, and Z3 is 69.3 ± 0.5 Ma (MSWD=0.18). LA-MC-ICP-MS analyses of five separate grains remain normally discordant, possibly an artefact of slightly inaccurate $^{207}\text{Pb}/^{206}\text{Pb}$ normalization with respect to the standard zircon 91500, although they overlap within error (Figure 5c and Table S6). The mean ^{206}Pb - ^{238}U age is 68.0 ± 2.5 Ma (MSWD=2.5) and, if plotted on a Tera-Wasserburg diagram, the lower intercept for plausible values of $^{207}\text{Pb}/^{206}\text{Pb}$ of common Pb is 66.3 ± 2.0 Ma (MSWD=2.0). Given this data set, the ID-TIMS Concordia age of 69.0 ± 0.3 Ma is likely to be the most accurate and precise, while remaining compatible with the LA-MC-ICP-MS data.

4.1.2. Tonalitic to Dioritic Magmatism, Nubra Valley

4.1.2.1. Sample P142, Tonalite-Diorite, Arganglas Range

[37] The Arganglas tonalite-diorite dominates the high ground northeast of the Nubra-Siachen

leucogranites. This unit was sampled in only one location due to the difficulty in accessing the elevated terrane that borders Tibet. At this location the diorite has a pl+hbl+bt+Kfs+qtz±cpx composition and appeared homogeneous. At its southwestern boundary the diorite was separated from the Nubra-Siachen leucogranites by the Arganglas fault, a steep northeast-dipping shear zone dominated by deformed marbles and pelites similar to that observed within the Nubra formation.

[38] U-rich fractions for sample P142 provide ID-TIMS age data of some complexity. Despite air abrasion of all zircon fractions, the analyses display variable ^{206}Pb - ^{238}U and ^{207}Pb - ^{235}U ages (Figure 4e, Tables S3 and S5). The data are consistent with inheritance in Z4, Z5, and possibly Z1, although the concordance of Z1 suggests a ^{206}Pb - ^{238}U age of 107.2 ± 0.5 Ma. In an attempt to resolve the age interpretation, ID-TIMS analysis of titanite and allanite were undertaken. Fractions T1 and A2 both display a large age error due to the significant uncertainty in the common lead corrections. By using a $^{207}\text{Pb}/^{204}\text{Pb}$ vs. $^{235}\text{Pb}/^{204}\text{Pb}$ isochron diagram, the analyses yield an age of 103.9 ± 5.9 Ma (MSWD = 0.19). Addition of Z1 to the isochron provides an age of 104.6 ± 5.9 Ma (MSWD = 0.30), and is essentially equivalent.

[39] As the ^{207}Pb - ^{235}U ages of T1 and A2 overlap with the age for Z1, and in view of the possibility of significant excess ^{206}Pb in allanite, it is appropriate to take the mean weighted age of all of the fractions, i.e., 107.0 ± 3.1 (MSWD = 0.85). This is taken as the most conservative age for sample P142 obtained by ID-TIMS. Results from the LA-MC-ICP-MS analysis offer similar age complexity (Figure 5d and Table S6). Six analyses on five grains provide a lower intercept of 107.7 ± 2.3 Ma (MSWD = 2.3), although the regression includes the reversely discordant grains P142-5 and P142-6. A more appropriate solution is the Concordant age of 108.6 ± 1.7 Ma (MSWD = 2.0) for grains P142-1 and P142-4. The lower uncertainty of these determinations is regarded as the best age estimate for this sample.

4.1.3. Discussion of Precollisional U-Pb Geochronology

[40] The Pakistan Karakoram terrane displays a complex precollisional and postcollisional history, reflecting abundant subduction-related magmatism, staurolite-, kyanite-, and sillimanite-grade metamorphism and voluminous crustal anatexis (Figure 9 and Table S8; Searle [1991], Searle and Tirrul [1991],

Fraser et al. [2001], Searle et al. [2010]). Conversely, relatively little is known about lower crustal processes that have operated within southern and southwestern Tibet from surface exposure because, in general, only upper crustal volcano-sedimentary units are exposed. Consequently, an examination of the geochemical and temporal evolution of the Eurasian margin within the eastern and western Karakoram crust can provide insight into processes that occurred in the unexposed lower crustal equivalent terrane of southern Tibet.

[41] Across the western Karakoram, detailed geochemical and geochronological analysis has revealed some heterogeneity at varying scales. In the Hindu Kush region precollisional, subduction-related, magmatic units predominate with only minor postcollisional leucogranite magmatism [e.g., Hildebrand et al., 1998, 2000]; across the western Karakoram, the Hunza region consists of a massive precollisional subduction-related granite batholith, intruded by several phases of postcollisional leucogranite dykes and minor plutons [Rex et al., 1988; Crawford and Searle, 1992; Fraser et al., 2001]. In the central and southern Karakoram, the Baltoro region displays numerous deformed precollisional diorite-granodiorite-amphibolite magmatic units [e.g., K2, Muztagh Tower, Hushe gneiss complexes; Rex et al., 1988; Searle et al., 1989, 1990, 2010] and a massive postcollisional Miocene crustal melt monzogranite to garnet two-mica leucogranite batholith, the Baltoro Plutonic unit [Parrish and Tirrul, 1989; Searle et al., 1989, 1992, 2010]. Searle and Tirrul [1991], Fraser et al. [2001], and Searle et al. [2010] have provided a detailed framework for the temporal evolution of the Baltoro region of the southern Pakistan Karakoram and suggest that, at a regional scale, the Karakoram lower-crust displays multiple phases of high-temperature sillimanite-grade metamorphism at 65 Ma. Critically, these studies excluded an analysis of the eastern Karakoram, in Ladakh, NW India, as the eastward continuation of the Baltoro Karakoram [Searle et al., 1998].

[42] In the eastern Karakoram, the earliest documented phase of magmatism is the tonalite-diorite orthogneiss of the Arganglas Range, Nubra Valley, (sample P142 108.6 ± 1.7 Ma), which is coeval with diorite orthogneiss petrogenesis in the Tangtse valley (sample P112 109.3 ± 1.8 Ma). Geochemically, these samples are equivalent to undated diorites within the Pangong Transpressional Zone at Muglib (sample P129) and are considered of comparable age. This middle Cretaceous granitoid suite records subduction-related magmatism along the Karakoram above a north-dipping subduction zone.

At this time, the south Asian margin was likely to have been an elevated and crust-thickened terrane comparable to the present-day Andes [Searle *et al.*, 1989, 1999].

[43] The eastern Karakoram precollision granitoids have protoliths that are geochemically and chronologically equivalent to the Hunza granites, Hushe gneiss, K2 gneiss, and Muztagh Tower hbl-bt granitoid gneiss of the Baltoro Karakoram to the northwest [e.g., Rex *et al.*, 1988; Searle *et al.*, 1989, 1990; Searle, 1991; Crawford and Searle, 1992]. The Cretaceous granitoids of the Baltoro intruded the Palaeozoic-early Mesozoic continental margin sediments of South Asia, the protolith of the Karakoram Metamorphic Complex, and resulted in a period of regional high temperature, low-pressure, metamorphism termed M0 by Fraser *et al.* [2001]. This event is equivalent to the M0 metamorphic event in the Hindu Kush [Hildebrand *et al.*, 2000].

[44] Our age data from the eastern Karakoram also constrains an important phase of magmatism during the Late Cretaceous between 82.7 ± 0.7 Ma (P28) and 69.0 ± 0.3 Ma (P139). These latter samples form part of a suite of granitoids that define a magmatic fractionation trend between monzodiorite and syenogranite. As discussed in section 3, the geochemistry of this suite suggests an evolved and complex history involving possible partial melting of amphibole-bearing rocks in the lower crust. This magmatic phase therefore reflects the prolonged closure of a back-arc basin between the Kohistan-Dras Arc and Karakoram terrane during the middle to Late Cretaceous. Fraser *et al.* [2001] defined the deformation and metamorphism associated with the collision and accretion of Kohistan onto the Karakoram terrane during the Late Cretaceous as D1 and M1-a (Figure 9).

[45] Treloar *et al.* [1989, 1996] suggested that closure of the Kohistan-Dras back-arc basin along the Shyok suture zone occurred at ~ 100 –85 Ma (K-Ar and Ar-Ar), prescribing an earlier cessation to back-arc magmatism than defined in this study. In addition, Jain and Singh [2008] obtained U-Pb SHRIMP ages of 76 ± 1 Ma from a mylonite from Tangtse and 68 ± 1 Ma age from the undeformed Tirit granodiorite. They suggested that these ages bracketed earliest shearing along the Karakoram fault. However, we suggest that their age for the mylonite represents a protolith age that predates the initiation of the Karakoram fault (similar to the 69.0 ± 0.3 Ma sample P139, this study). The Tirit granodiorite in the Nubra valley is part of the Ladakh batholith south of the Karakoram fault and

thus is in no way related to deformation associated with strike-slip shearing.

[46] The eastern Karakoram Late Cretaceous suite lies solely within the Pangong Transpressional Zone, an exhumed lower crustal portion of the Karakoram crust. We correlate this magmatic event as similar to timing of subduction-related magmatism in the Hunza granodiorites, the K2 gneiss, Hushe gneiss, and the earliest component of the Masherbrum migmatites in the Baltoro region of the central Karakoram [Searle *et al.*, 1989, 1990; Searle, 1991; Crawford and Searle, 1992].

[47] In summary, the middle to Late Cretaceous granitoid suite of the eastern Karakoram displays a temporal and geochemical correlation with granitoids across the western, central, and southern Karakoram of Pakistan, suggesting that that the regions were part of the same geological terrane.

4.2. U-Pb Geochronology of Postcollisional Magmatism

[48] Leucogranite sheets, domes, and dykes are ubiquitous within the Nubra-Siachen Valley and the PTZ. Sample localities and field relationships are shown in Figures 1–3. The PTZ consists of sheets and dykes that locally coalesced to supply magmatic units at higher structural levels, such as the Nubra-Siachen leucogranites. As outlined in the introduction, controversy remains over whether these leucogranites were derived either: (1) as a result of shear heating during movement along the Karakoram fault [Lacassin *et al.*, 2004; Valli *et al.*, 2007, 2008; Weinberg and Mark, 2008], or (2) from regional melting along the Karakoram batholith prior to initiation of the Karakoram fault [Searle, 1996; Phillips *et al.*, 2004; Phillips and Searle, 2007; Searle and Phillips, 2004, 2007]. Compositionally, the suite consists of $qtz + kfs + pl + bt \pm ms \pm grt$ leucogranites, $pl + qtz + Kfs + bt$ migmatite leucosomes and megacrystic K-feldspar leucogranites with the assemblage $kfs + qtz + pl + bt$. Constraining the age of leucogranite emplacement within the eastern Karakoram forms an essential part of the discussion of formation offset along the Karakoram fault because a correlation with the Baltoro Plutonic Unit, in the southern Karakoram of Pakistan, has been previously inferred following U-Pb dating, microstructural analysis and combined field and satellite mapping [Searle, 1996; Searle *et al.*, 1998; Phillips *et al.*, 2004; Searle and Phillips, 2007; Phillips and Searle, 2007; Phillips, 2008; Jain and Singh, 2008].

4.2.1. Sample P175, Leucogranite Sheet, Darbuk Valley

[49] Sample P175, a K-feldspar megacrystic mica leucogranite, represents an undeformed broad intrusive sheet preserved between Darbuk and Shyok villages, in the Pangong Transpressional Zone. Similar megacrystic leucogranites are evident within the Nubra valley and generally appear to form the outer sheath of the leucogranite complex. When calculated with the Stacey-Kramers model lead, analyses P175 Z1a, Z1b, and Z2 plot with slight reverse discordance, a relationship not normally observed for zircon (Figure 4j and Table S4). When corrected for common lead by the use of K-feldspar rather than the Stacey-Kramers model, the reversely discordant fractions are displaced toward Concordia suggesting a more appropriate correction. Using this, the mean weighted ^{207}Pb - ^{235}U age of 22.5 ± 2.1 Ma for all zircon analyses is regarded to be most representative of the crystallization age for this sample. Minor inheritance could explain the U-Pb systematics for Z1b or equally lead loss may be important in Z1a and Z2. A rutile analyses P175 R1 carries a large error in common lead using measured K-feldspar and plots with normal discordance. The rutile ID-TIMS ^{206}Pb - ^{238}U age of 12.8 ± 2.1 Ma reflects a closure temperature ~ 660 – 700°C [Scott and St-Onge, 1995; Pidgeon et al., 1996; Frost et al., 2000] and is compatible with a ^{40}Ar - ^{39}Ar age of 11.40 ± 0.01 Ma from muscovite in the mylonitic Tangtse granite sample of Searle et al. [1998] and the two-phase cooling of the PTZ defined by Dunlap et al. [1998].

[50] Laser ablation multicollector-inductively coupled plasma-mass spectrometry analyses on four separate grains provide an improved age resolution for P175 but suggest a complexity similar to that observed in the ID-TIMS study (Figure 5e and Table S7). Grains P175-3 to P175-5 lie along Concordia between ~ 20 and 22 Ma. Although grain P175-5 lies on Concordia, it is younger than two other concordant analyses. Given the high U content for P175-5, it is possible that the grain has suffered Pb-loss in its outer surface, making this analysis less reliable. Furthermore, sample P175-1 is considered unreliable because it displays reverse discordance. The age for P175 is taken as the more robust Concordia age of 21.7 ± 0.5 Ma (MSWD=0.15) for grains P175-3 and P175-4, an age compatible but more precise with that derived by ID-TIMS.

4.2.2. Sample P113, Migmatite Leucosome, Tangtse Valley

[51] The melt portion of the migmatite complex is a pl + qtz + Kfs + bt leucosome. An age for this sample thus constrains in situ melting of the protolith. ID-TIMS analysis of two zircon fractions from the migmatitic leucosome yields ages that are concordant within error (Figure 4d, Table S3 and S5). The Concordia ^{206}Pb - ^{238}U age of fractions P113 Z1 and Z3 is 17.3 ± 0.1 Ma (MSWD=0.02). Fraction P113 T2 plots discordantly with an elevated ^{207}Pb - ^{235}U age and is not used in the Concordia calculation.

[52] The LA-MC- ICP-MS analysis for P113 suggests some complexity in the age history of the leucosome (Figures 5f–5h and Table S7). Thirteen analyses on seven grains provide a ^{206}Pb - ^{238}U and ^{207}Pb - ^{235}U regression of low precision (16.5 ± 1.4 Ma, MSWD=15), chiefly due to the difficulty in resolving the common Pb for low laser fluence measurements. Examination of ^{206}Pb - ^{238}U and ^{207}Pb - ^{235}U regressions for individual grains indicates that the apparent complexity deconvolutes into two age groups: grains P113-1 and P113-2 provide a regression age of 13.4 ± 0.7 Ma (MSWD=0.14, Figure 5f), while grains P113-3 to P113-7 reduce to 17.5 ± 1.4 Ma (MSWD=3.2, Figure 5g). Given that lead-loss is unlikely to explain the age distribution, the distinct age data may reflect discrete zircon growth stages during crystallization phases at ~ 17 Ma and ~ 13 Ma. Certainly, there is evidence for melting within the Pangong Transpressional Zone at ~ 13 Ma; age data for sample P67 supports late-stage pegmatitic intrusion at 12.72 ± 0.04 Ma, with ~ 13 – 14 Ma aged dyking in both the PTZ (sample P8; Phillips et al. [2004]) and the Nubra valley (P37; Phillips et al. [2004]).

[53] For grains P113-3 to P113-7, an improved age for leucosome melting can be resolved by determining an appropriate Concordia age (Figure 5h). High fluence data for grains P113-5b and P113-7b lie on Concordia, with grain P113-3b plotting slightly to the right of Concordia and with an elevated ^{206}Pb - ^{238}U ratio suggesting slight inheritance. Discounting P113-3b, in situ melting is thus constrained by a ^{206}Pb - ^{238}U and ^{207}Pb - ^{235}U Concordia age for grains P113-5b and P113-7b of 17.4 ± 0.4 Ma (MSWD=0.31), an age in excellent agreement with the ID-TIMS Concordia age for P113.

4.2.3. Sample P46, Leucogranite Pluton, Muglib

[54] Sample P46 derives from a kilometer-sized leucogranite pluton in the Tangtse valley and is

bounded by the Muglib Migmatite Complex, adjacent to, and cut by, the Pangong fault strand. Granite emplacement-related fabrics wrap around the domal-shaped pluton [Searle *et al.*, 1998] and these fabrics are cut and overprinted by vertical dextral strike-slip fabrics related to shear strain along the fault. Strain, associated with slip on the fault, is evident by slip-parallel foliations, which decrease markedly away from the fault. The structural relation between the Muglib dome and the Pangong fault strand suggest that an age for the pluton provides a maximum age for the initiation of this strand of the Karakoram fault.

[55] U-rich heavy mineral separates for P46 were dominated by igneous titanite and apatite. Some slender laths of zircon were present in the cores of apatite although their small size ($< 10 \mu\text{m}$) precluded their use. Four titanite fractions of varying grain morphology and size were analysed via ID-TIMS (Figure 4g, Table S4 and S5). All of the fractions were corrected for common lead using measured feldspar and are concordant within error, yielding a weighted mean ^{206}Pb - ^{238}U age of $15.1 \pm 0.6 \text{ Ma}$ (MSWD = 2.5). The concordant age suggests negligible discrepancy between ductile deformation on the Tangtse and Pangong strands (by comparison to samples P1 and P11 [Phillips *et al.*, 2004]) and implies that strike-slip shearing and subsequent transpressional exhumation initiated soon after 15 Ma.

4.2.4. Sample P109, Leucogranite Dyke, Tangtse Valley

[56] Throughout the Tangtse valley, a complex network of fine- to medium-grained leucogranite dyking is evident. Following detailed mapping, sample P109 is interpreted as being representative of the oldest phase of dyking exposed within the Pangong Transpressional Zone. In combination with the late-stage pegmatite (sample P67, this study) and cross-cutting dykes (samples P8 and P11 [Phillips *et al.*, 2004]), sample P109 helps to constrain the full temporal evolution of dyking within the transpressional zone. Age data for fractions P109 Z2, Z3, Z4, and Z6 provide a discordant non-linear array between ~ 16 and 23 Ma when reduced using the Stacey-Kramers model for common Pb correction (Figure 4i and Table S4). In the absence of other mineral analyses, the mixed age array can be regressed in an attempt to estimate the crystallization age from the lower intercept. Assuming lead loss for P109 Z4, regression through the remaining analyses provides

an age of $14.6 \pm 1.1 \text{ Ma}$ (MSWD = 0.83), which is within error of the age for the concordant dyke phase (P11 [Phillips *et al.*, 2004]) within the Tangtse shear zone.

[57] The LA-MC- ICP-MS analysis for P109 provides a data set that is difficult to resolve (Figure 5i and Table S7). Eight analyses from five grains suggest markedly variable common Pb and U concentrations. A regression for the entire data set provides a lower intercept of $16.4 \pm 4.3 \text{ Ma}$ (MSWD = 5.6), the poor resolution due, in part, to the low levels of ^{207}Pb and the large associated measurement errors. A significant controlling factor in the imprecision is the reverse discordance for samples P109-1ai, 1aii, 2, 3, and 5. Because the ^{206}Pb - ^{238}U ages of three of the samples are within error (P109-1aii, bii, 5), a weighted mean age of $15.5 \pm 0.7 \text{ Ma}$ (MSWD = 2.4) provides a cautious age estimate via in situ measurements. Without further microanalytical or ID-TIMS analyses, this latter age for P109 is taken as best estimate for the timing of early dyking within the PTZ. The age is within error of the ID-TIMS estimate for P109 and in close agreement for the nearby P11 dyke phase ($15.2 \pm 0.4 \text{ Ma}$ [Phillips *et al.*, 2004]).

4.2.5. Sample P67, Leucogranite Dyke, Darbuk Valley

[58] This sample lies within the Karakoram Fault ductile shear zone immediately SW of the Pangong fault strand near Shyok village. It is a leucogranite pegmatite and exhibits a vague slip-parallel foliation provided by alignment of rare mica. Within the shear zone, the pegmatite suite is observed to cross-cut other leucogranite intrusives. An age for sample P67 indicates the timing of late-stage pegmatitic intrusion within the Pangong Transpressional Zone. Fractions P67 Z1 and Z4 are concordant within error and yield a mean weighted ^{206}Pb - ^{238}U age of $12.72 \pm 0.04 \text{ Ma}$ (MSWD = 0.01; Figure 4h and Table S4). This provides a minimum age for fault initiation and subsequent transpression along the Pangong fault strand at the exposed structural level.

[59] The LA-MC- ICP-MS data for P67 supports the ID-TIMS interpretation (Figure 5j and Table S7). Four analyses on three grains were carried out with one low fluence analysis of poor resolution (P67-3a). The three remaining data provide a ^{206}Pb - ^{238}U and ^{207}Pb - ^{235}U regression of $13.1 \pm 0.3 \text{ Ma}$ (MSWD = 0.62), in close agreement with the preferred ID-TIMS age.

4.3. Discussion of Postcollisional U-Pb Geochronology

[60] Garnet two-mica leucogranite magmatism dominates the postcollisional crustal magmatism in the eastern Karakoram, similar to the Baltoro region west of the Karakoram Fault. Geochemical analysis of the ~22–12 Ma leucogranite suite indicates that these leucogranites were formed by dehydration melting of a biotite-rich pelitic source in response to elevated thermal gradients associated with crustal thickening. The chronology of the comagmatic leucogranite suite of the eastern Karakoram suggests that intrusion proceeded in the following order of emplacement:

- (1) Large K-feldspar megacrystic leucogranite sheets (P175; 21.7 ± 0.5 Ma)
- (2) Tonalitic leucosome (P113; 17.4 ± 0.4 Ma)
- (3) Biotite leucogranite sheets (P38; 15.9 ± 0.1 Ma); Garnet two-mica leucogranite sheets and early dykes (P1; 15.6 ± 0.75 Ma, P11; 15.6 ± 0.5 Ma, P109; 15.5 ± 0.7 Ma); Biotite leucogranite domes (P46; 15.1 ± 0.6 Ma)
- (4) Late garnet two-mica leucogranite dykes (P37; 13.7 ± 0.3 Ma, P8; 13.7 ± 0.3 Ma)
- (5) Late-stage garnet biotite leucogranitic pegmatites (P67; 12.72 ± 0.04 Ma)

[61] These magmatic phases correlate closely with those of the ~26–13 Ma Baltoro plutonic unit (BPU) in the Pakistan Karakoram (Figure 9 and Table S8; Parrish and Tirrul [1989], Searle et al. [1989, 1992], Fraser et al. [2001], and Searle et al. [2010]). The elongate, 100 km long BPU is the most extensive magmatic unit within the Karakoram and trends approximately WNW-ESE, abutting and offset by the Karakoram fault near the Siachen glacier in NW India. The BPU is composed of K-feldspar megacrystic leucogranite sheets, biotite-muscovite leucogranite sheets, garnet two-mica monzogranite sheets and dykes, and garnet ± two-mica leucogranite pegmatites and are geochemically and isotopically equivalent to those in the eastern Karakoram. Associated with the intrusion of the BPU is a localised contact metamorphism event D3/M3 associated with the Mitre sillimanite–andalusite bearing contact metamorphic aureole along the northern margin of the Baltoro granite [e.g., Searle et al., 1989, 1992, 2010]. Streule et al. [2009] have shown that sillimanite-grade metamorphism within the Pangong Metamorphic Complex, adjacent to the Karakoram fault in the eastern Karakoram, occurred at 108 ± 0.6 Ma, equating to M0 of Fraser et al. [2001] and thus significantly predates fault motion. Subsequent P-T conditions at 585–605°C and

6.1–7.3 kbar, reflecting 20–25 km of burial, demonstrates that prolonged precollisional thickening of the South Asian margin was widespread across the Karakoram [e.g., Searle et al., 2010].

[62] Our new geochemical and U-Pb geochronological data show that the eastern Karakoram leucogranites are likely comagmatic with the Baltoro granite batholith in the Pakistan Karakoram [e.g., Parrish and Tirrul, 1989; Searle et al., 1989, 1992, 2010; Fraser et al., 2001]. This supports previous suggestions that the postcollisional Miocene Baltoro-type granite batholith extends at least from the Hispar glacier-Snow Lake region through the main Baltoro granites to the Siachen-Nubra granites and southeast through the Pangong Range [Searle et al., 1998; Phillips et al., 2004; Searle and Phillips, 2007]. The Baltoro granites south and west of the Karakoram fault are largely undeformed whereas, along the Pangong range, subsequent right-lateral shear fabrics formed during later strike-slip ductile shearing have been superimposed onto earlier magmatic fabrics.

5. Granite Petrogenesis, Metamorphism and the Evolution of the Eastern Karakoram Crust: Implications for the Evolution of the Karakoram Fault

[63] New coupled LA-MC-ICP-MS and ID-TIMS U-Pb age data, combined with new geochemical and isotopic data demonstrate that both the precollision and postcollision leucogranite units of the Karakoram batholith were continuous from the Baltoro region west of the fault to the Siachen-Nubra-Pangong region of the eastern Karakoram, east of the fault. The earliest record of magmatism within the eastern Karakoram is a ~108 Ma orthogneiss and is equivalent to the Broad Peak, K2 gneiss, and Muztagh Tower units of the central Karakoram. Late Cretaceous magmatism is recorded by ~82–69 Ma diorites that record prolonged closure of a back-arc basin between the Kohistan-Dras Arc and the South Asian margin.

[64] Early-middle Miocene (~22–13 Ma) leucogranite magmatism dominates the postcollisional crustal melting in the eastern Karakoram, and equate to the ~26–13 Ma Baltoro granites of the Pakistan Karakoram [Searle et al., 2010].

[65] It has been suggested that leucogranite magmatism and metamorphism in the eastern Karakoram was a result of right-lateral shearing along the Karakoram fault and equates to syn-kinematic

magmatism and shearing in Zhaxigang to the south-east [Lacassin *et al.*, 2004; Valli *et al.*, 2007, 2008; LeLoup *et al.*, 2011; Boutonnet *et al.*, 2012]. However, in the eastern Karakoram it is evident that metamorphism in the Pangong range predates shearing [Streule *et al.*, 2009] and was more regional in extent, extending a significant distance west of the fault into the southern Karakoram metamorphic complex of Pakistan [Searle and Tirrul, 1991]. Furthermore, our field and microstructural analysis [Phillips *et al.*, 2004; Phillips and Searle, 2007] implies that ductile C-S fabrics were superimposed onto already crystallized granites at Tangtse and along strike in the Nubra valley. The U-Pb crystallization age of the granites may therefore only provide a maximum age of initiation of strike-slip shear along the fault.

[66] With regard to the geochronologic work in the Zhaxigang region, Lacassin *et al.* [2004] and Valli *et al.* [2007, 2008] suggest that mylonites are late Oligocene in age and relate these fabrics to activity on the Karakoram Fault. Unfortunately, as documented by Zhang *et al.* [2011], the dated mylonites were formed in the footwall of a regionally extensive detachment fault that is cut by the Karakoram fault and therefore do not relate to the Karakoram Fault itself. This observation, in conjunction with U-Pb SHRIMP dating of the Ayilari granite near Zhaxigang, from the hanging wall of the detachment [Wang *et al.*, 2009, 2012], shows the Karakoram fault was not active in the region until ~13 Ma in this region.

[67] The data presented here strongly imply that the eastern Karakoram leucogranites were continuous with the Baltoro leucogranites and that these were all emplaced in a regional setting and distributed regionally well away from the fault, rather than being entirely spatially related to the fault as expected if syn-kinematic and coeval with faulting. This corroborates the suggestion by Searle *et al.* [1998] and Phillips *et al.* [2004] that the magmatic units of the eastern and central Karakoram were emplaced, cooled, and subsequently offset by the Karakoram fault and can only provide a maximum age of faulting. As such the magmatic units provide temporal and spatial constraints on the initiation and evolution of the Karakoram fault and provide direct evidence that the fault could not have accommodated lateral offset in this region prior to ~16 Ma. Phillips *et al.* [2004] suggest that the eastern Karakoram leucogranites provide a maximum offset limit of 150 km with a consequent long-term average slip rate of less than 10 mm/yr. The data support the idea that deformation, metamorphism,

and plutonism along the Karakoram fault was not synchronous as claimed by several previous workers. Metamorphism along the fault is Late Cretaceous and unrelated to the fault; magmatism spans over 100 Ma with postcollisional leucogranites spanning 22–13 Ma, the exact period of the undeformed Baltoro granite magmatism away from fault.

Acknowledgments

[68] We gratefully acknowledge support from NERC (grant NER/S/A/2000/03515 to RJP and grant NER/K/S/2000/951 to MPS). Matt Horstwood is thanked for discussions regarding the LA-MC-ICP-MS data. Reviews by Alexander Robinson and an anonymous reviewer greatly improved the manuscript. Louis Derry is thanked as editor.

References

- Allègre, C. J., and D. B. Othman (1980), Nd-Sr isotopic relationship in granitoid rocks and continental crust development: a chemical approach to orogenesis, *Nature*, **286**, 335–346.
- Boutonnet, E., P. H. LeLoup, N. Arnaud, J.-L. Paquette, W. J. Davis, and K. Hattori (2012), Synkinematic magmatism, heterogeneous deformation, and progressive strain localization in a strike slip shear zone. The case of the right-lateral Karakoram fault, *Tectonics*, **31**, TC4012, doi:10.1029/2011TC003049.
- Burrard, S. (1929), The Mountains of the Karakoram: A defence of the existing nomenclature, *Geogr. J.*, **LXXIV**(3), 277–284.
- Crawford, M. B. (1988), Leucogranites of the NW Himalaya, PhD thesis, University of Leicester, UK.
- Crawford, M. B., and M. P. Searle (1992), Field relationships and geochemistry of pre-collisional (India-Asia) granitoid magmatism in the central Karakoram, *Tectonophysics*, **206**, 171–192.
- Crawford, M. B., and B. F. Windley (1990), Leucogranites of the Himalaya / Karakoram: implications for magmatic evolution within collisional belts and the study of collision related leucogranite petrogenesis, *J. Volcanol. Geothermal. Res.*, **44**, 1–19.
- Deniel, C., P. Vidal, and A. Fernandez (1987), Isotopic study of the Manaslu granite (Himalaya, Nepal) – inferences on the age and source of Himalayan leucogranites, *Contrib. Min. Pet.*, **96**, 78–92.
- Dunlap, W. J., R. Weinberg, and M. P. Searle (1998), Karakoram fault zone rocks cool in two phases, *J. Geol. Soc. Lond.*, **155**, 903–912.
- Fraser, J. E., M. P. Searle, R. R. Parrish, and S. R. Noble (2001), Chronology of deformation, metamorphism, and magmatism in the southern Karakoram Mountains, *Geol. Soc. Am. Bull.*, **113**, 1443–1455.
- Frost, B. R., K. R. Chamberlain, J. C. Schumacher, D. J. Scott, and D. E. Moser (2000), Sphene (titanite); phase relations and role as a geochronometer, *Chem. Geol.*, **172**, 131–148.
- Hildebrand, P. R., S. R. Noble, M. P. Searle, and R. R. Parrish (1998), Tectonic significance of 24 Ma crustal melting in the eastern Hindu Kush, Pakistan, *Geology*, **26**, 865–960.
- Hildebrand, P. R., S. R. Noble, M. P. Searle, D. J. Waters, and R. R. Parrish (2000), An origin for an active mountain range:

- geology and geochronology of the eastern Hindu Kush, Pakistan, *Geol. Soc. Am. Bull.*, *113*, 45–76.
- Harris, N. B. W., M. Ayres, and J. Massey (1995), Geochemistry of granitic melts produced during the incongruent melting of muscovite - implications for the extraction of Himalayan leucogranite magmas, *J. Geophys. Res.*, *100*(B8), 15767–15777.
- Harris, N., and S. Inger (1992), Trace element modelling of pelite derived granites, *Contrib. Min. Pet.*, *104*, 46–56.
- Hollister, L. S., and M. L. Crawford (1986), Melt-enhanced deformation: A major tectonic process, *Geology*, *14*, 558–561.
- Inger, S., and N. Harris (1993), Geochemical constraints on leucogranite magmatism in the Langtang valley, Nepal Himalaya, *J. Petrol.*, *34*, 345–368.
- Jain, A. K., and S. Singh (2008), Tectonics of the southern Asian Plate margin along the Karakoram Shear Zone: Constraints from field observations and U-Pb SHRIMP ages, *Tectonophysics*, *451*, 186–205.
- Lacassin, R., F. Valli, N. Arnaud, P. H. Leloup, J. L. Paquette, L. Haibing, P. Tapponnier, M.-L. Chevalier, S. Guillot, G. Mahéo, and X. Zhiqin (2004), Large-scale geometry, offset and kinematic evolution of the Karakoram fault, Tibet, *Earth Planet. Sci. Lett.*, *219*, 255–269.
- Leech, M. (2008), Does the Karakoram fault interrupt mid-crustal channel flow in the western Himalaya? *Earth Planet. Sci. Lett.*, *276*, 314–322.
- Leloup, P. H., E. Boutonnet, W. J. Davis, and K. Hattori (2011), Long-lasting intracontinental strike-slip faulting: new evidence from the Karakoram shear zone in the Himalayas, *Terra Nova*, *23*, 92–99.
- Mahéo, G., J. Blichert-Toft, C. Pin, S. Guillot, A. Pêcher (2009), Partial melting of mantle and crustal sources beneath South Karakoram, Pakistan: Implications for the Miocene geodynamic evolution of the India-Asia convergence zone, *J. Petrol.*, *50*, 427–449, doi:10.1093/ptrology/egp006.
- Miller, C., R. Schuster, U. Klotzli, V. Mair, W. Frank, and F. Purtscheller (1999), Post-collisional potassic and ultrapotassic magmatism in SW Tibet: Geochemical, Sr-Nd-Pb-O constraints for mantle source characteristics and petrogenesis, *J. Petrol.*, *40*, 1399–1424.
- Najman, Y., E. Appel, M. Boudagher-Fadel, P. Brown, A. Carter, E. Garzanti, L. Godin, J. Han, U. Liebke, G. Oliver, R. Parrish, G. Vezzoli (2010), Timing of India-Asia collision: Geological, biostratigraphic, and palaeomagnetic constraints, *J. Geophys. Res.*, *115*, B12416, doi: 10.1029/2010JB007673.
- Parrish, R. R. (2009), Comment on: “Does the Karakoram fault interrupt mid-crustal channel flow in the western Himalaya?” by Mary L. Leech, *Earth and Planetary Science Letters* *276* (2008) 314–322, *Earth Planet. Sci. Lett.*, *286*, 586–588, doi:10.1016/j.epsl.2009.05.038.
- Parrish, R. R., and R. Tirrul (1989), U-Pb age of the Baltoro granite, north-west Himalaya, and implications for zircon inheritance and U-Pb systematics, *Geology*, *17*, 1076–1079.
- Petford, N., and M. P. Atherton (1992), Granitoid emplacement and deformation along a major crustal lineament: The Cordillera Blanca, Peru, *Tectonophysics*, *205*, 171–185.
- Phillips, R. J. (2008), Geological map of the Karakoram fault zone, Eastern Karakoram, Ladakh, NW Himalaya, *J. Maps*, v.2008, 21–37.
- Phillips, R. J., R. R. Parrish, and M. P. Searle (2004), Age constraints on ductile deformation and long-term slip rates along the Karakoram fault zone, Ladakh, *Earth Planet. Sci. Lett.*, *226*, 305–319.
- Phillips, R. J., and M. P. Searle (2007), Macrostructural and microstructural architecture of the Karakoram fault: Relationship between magmatism and strike-slip faulting, *Tectonics*, *26*, TC3017, doi:10.1029/2006TC00946.
- Pidgeon, R. T., D. Bosch, and O. Bruguier (1996), Inherited zircon and titanite U-Pb systems in an archaean syenite from southwestern Australia: Implications for U-Pb stability of titanite, *Earth Planet. Sci. Lett.*, *141*, 187–198.
- Rex, A. J., M. P. Searle, R. Tirrul, M. B. Crawford, D. J. Prior, D. C. Rex, and A. Barnicoat (1988), The geochemical and tectonic evolution of the central Karakoram, North Pakistan, *Phil. Trans. R. Soc. Lond.*, *A326*, 229–255.
- Robinson, A. C., M. Ducea, T. J. Lapen (2012), Detrital zircon and isotopic constraints on the crustal architecture and tectonic evolution of the northeastern Pamir, *Tectonics*, *31*, TC2016, doi:10.1029/2011TC003013.
- Rowley, D. B. (1996), Age of initiation of collision between India and Asia: A review of stratigraphic data, *Earth Planet. Sci. Lett.*, *145*, 1–13.
- Saunders, A. D., M. J. Norry, and J. Tarney (1988), Origin of MORB and chemically-depleted mantle reservoirs: trace element constraints, in *Oceanic and Continental Lithosphere: Similarities and Differences*, J. Pet., Special Volume, edited by M. A. Menzies and K. G. Cox, 415–455.
- Schärer, U., P. Copeland, T. M. Harrison, and M. P. Searle (1990), Age, cooling history and origin of postcollisional leucogranites in the Karakoram batholith, a multisystem isotope study, *J. Geol.*, *98*, 233–251.
- Schwab, M., L. Ratschbacher, W. Siebel, M. McWilliams, V. Minaev, V. Lutkov, F. Chen, K. Stanek, B. Nelson, W. Frisch, J. L. Wooden (2004), Assembly of the Pamirs: Age and origin of magmatic belts from the southern Tien Shan to the southern Pamirs and their relation to Tibet, *Tectonics*, *23*, TC4002, doi:10.129/2003TC001583.
- Scott, D. J., and M. R. St-Onge (1995), Constraints on Pb closure temperature in titanite based on rocks from the Ungava orogen, Canada: implications for U-Pb geochronology and P-T-t path determinations, *Geology*, *23*, 1123–1126.
- Searle, M. P. (1991), *Geology and Tectonics of the Karakoram Mountains*, John Wiley and Sons, Chichester.
- Searle, M. P. (1996), Geological evidence against large-scale pre-Holocene offsets along the Karakoram fault: Implications for the limited extrusion of the Tibetan Plateau, *Tectonics*, *15*, 171–186.
- Searle, M. P., M. B. Crawford, and A. J. Rex (1992), Field relations, geochemistry, origin and emplacement of the Baltoro granite, central Karakoram, *R. Soc. Edin. Trans.*, *83*, 519–538.
- Searle, M. P., J. R. Elliott, R. J. Phillips, S. L. Chung (2011), Crustal-lithospheric structure and continental extrusion of Tibet, *J. Geol. Soc. Lond.*, *168*, 633–672. doi:10.1144/0016-76492010-139.
- Searle, M. P., M. A. Khan, J. E. Fraser, and S. J. Gough (1999), The tectonic evolution of the Kohistan-Karakoram collision belt along the Karakoram Highway transect, north Pakistan, *Tectonics*, *18*, 929–949.
- Searle, M. P., R. R. Parrish, K. V. Hodges, A. Hurford, M. W. Ayres, and M. J. Whitehouse (1997), Shisha Pangma leucogranite, south Tibetan Himalaya: field relations, geochemistry, age, origin, and emplacement, *J. Geol.*, *105*, 295–317.
- Searle, M. P., R. R. Parrish, A. V. Thow, S. R. Noble, R. J. Phillips, D. J. Waters (2010), Anatomy, age and evolution of a collisional mountain belt: the Baltoro granite batholith and Karakoram Metamorphic Complex, Pakistani Karakoram, *J. Geol. Soc. Lond.*, *167*, 183–202. doi:10.1144/0016-76492009-043.

- Searle, M. P., R. R. Parrish, R. Tirrul, and D. C. Rex (1990), Age of crystallisation and cooling of the K2 gneiss in the Baltoro Karakoram, *J. Geol. Soc. Lond.*, *147*, 603–606.
- Searle, M. P., and R. J. Phillips (2007), Relationships between right-lateral shear along the Karakoram Fault and metamorphism, magmatism, exhumation and uplift: evidence from the K2 - Gasherbrum – Pangong ranges, North Pakistan and Ladakh, *J. Geol. Soc. Lond.*, *164*, 439–450.
- Searle, M. P., and R. J. Phillips (2009), Comment on: "Does the Karakoram fault interrupt mid-crustal channel flow in the western Himalaya?" by Mary L. Leech, *Earth and Planetary Science Letters* *276* (2008) 314–322 Discussion, *Earth Planet. Sci. Lett.*, *286*, 589–591, doi:10.1016/j.epsl.2009.05.036.
- Searle, M. P., A. J. Rex, R. Tirrul, D. C. Rex, A. Barnicoat, and B. F. Windley (1989), Metamorphic, magmatic and tectonic evolution of the central Karakoram in the Biafo-Baltoro-Hushe regions of northern Pakistan, *Geol. Soc. Am. Spec. Pap.*, *232*, 47–73.
- Searle, M. P., and R. Tirrul (1991), Structural and thermal evolution of the Karaoram crust, *J. Geol. Soc. Lond.*, *148*, 65–82.
- Searle, M. P., R. F. Weinberg, and W. J. Dunlap (1998), Transpressional tectonics along the Karakorum fault zone, northern Ladakh: constraints on Tibetan extrusion, in *Continental Transpressional and Transtensional Tectonics: Geol. Soc. London Spec. Pub.*, vol. *135*, edited by R. E. Holdsworth et al., 307–326.
- Streule, M. J., R. J. Phillips, M. P. Searle, D. J. Waters, M. S. A. Horstwood (2009), Evolution and chronology of the Pangong Metamorphic Complex adjacent to the Karakoram Fault, Ladakh: constraints from thermobarometry, metamorphic modelling and U-Pb geochronology, *J. Geol. Soc. Lond.*, *166*, 919–932. doi:10.1144/0016-76492008-117.
- Tarney, J., and C. E. Jones (1994), Trace element geochemistry of orogenic igneous rocks and crustal growth models, *J. Geol. Soc. Lond.*, *151*, 855–868.
- Thow, A. (2004), Tectonic, Metamorphic and Magmatic Evolution of the Central Karakoram Crust, Northern Pakistan, PhD thesis, University of Oxford, UK.
- Tommasi, A., A. Vouchez, L. A. D. Fernandes, and C. C. Porcher (1994), Magma-assisted strain localization in an orogen-parallel transcurrent shear zone of southern Brazil, *Tectonics*, *13*, 421–437.
- Treloar, P. J., M. G. Petterson, M. Q. Jan, and M. A. Sullivan (1996), A re-evaluation of the stratigraphy and evolution of the Kohistan Arc sequence, Pakistan Himalaya; implications for magmatic and arc-building processes, *J. Geol. Soc. Lond.*, *153*, 681–693.
- Treloar, P. J., D. C. Rex, P. G. Guise, M. P. Coward, M. P. Searle, B. F. Windley, M. G. Petterson, M. Q. Jan, and I. W. Luff (1989), K-Ar and Ar-Ar geochronology of the Himalayan collision in NW Pakistan: constraints on the timing of suturing, deformation, metamorphism and uplift, *Tectonics*, *8*, 881–909.
- Valli, F., N. Arnaud, P. H. Leloup, E. R. Sobel, G. Mahéo, R. Lacassin, S. Guillot, H. Li, P. Tapponnier, and Z. Xu (2007), Twenty million years of continuous deformation along the Karakorum fault, western Tibet: A thermochronological analysis, *Tectonics*, *26*, TC4004, doi:10.1029/2005TC001913.
- Valli, F., P. H. Leloup, J.-L. Paquette, N. Arnaud, H. Li, P. Tapponnier, R. Lacassin, S. Guillot, D. Liu, E. Deloule, Z. Xu, and G. Mahéo (2008), New U-Th/Pb constraints on timing of shearing and long-term slip-rate on the Karakorum fault, *Tectonics*, *27*, TC5007, doi:10.1029/2007TC002184.
- Vauchez, A., S. Pacheco Neves, A. Tommasi (1997), Transcurrent shear zones and magma emplacement in Neoproterozoic belts of Brazil, in *Granite: From Segregation of Melt to Emplacement Fabrics*, edited by J. L. Bouchez, et al., Kluwer Academic Publishers, 275–294.
- Vidal, P., A. Cocherie, and P. Le Fort (1982), Geochemical investigations of the origin of the Manaslu leucogranite (Himalaya, Nepal), *Geochim. et Cosmochim. Acta*, *46*, 2279–2292.
- Wang, S., X. Fang, Q. Lai, D. Zheng, Y. Wang (2009), New radiometric dating constrains the time for initiation of the Karakorum fault zone (KFZ), SW Tibet, *Tectonophysics*, *475*, 503–513.
- Wang, S., C. Wang, R. J. Phillips, M. A. Murphy, Y. Yue (2012), Small-scale offset of the Karakoram Fault constrained by LA-ICP-MS U-Pb dating of displaced geological markers, *Earth Planet. Sci. Lett.*, doi: 10.1016/j.epsl.2012.05.037.
- Weinberg, R., W. J. Dunlap, and M. Whitehouse (2000), New field, structural and geochronological data from the Shyok and Nubra valleys, northern Ladakh: linking Kohistan to Tibet, in *Tectonics of the Nanga Parbat Syntaxis and the Western Himalaya.*, vol. *170*, edited by M. A. Khan, P. J. Treloar, M. P. Searle, M. Q. Jan (eds.) Geol. Soc. London Spec. Pub., 253–275.
- Weinberg, R. F., and G. Mark (2008), Magma migration, folding, and disaggregation of migmatites in the Karakoram Shear Zone, Ladakh, NW India, *Geol. Soc. Am. Bull.*, *120*, 994–1009.
- Weinberg, R. F., G. Mark, and H. Reichardt (2009), Magma ponding in the Karakoram shear zone, Ladakh, NW India, *Geol. Soc. Am. Bull.*, *121*, 278–285.
- Weinberg, R., and M. P. Searle (1998), The Pangong Injection Complex, Indian Karakoram: a case of pervasive granite flow through hot viscous crust, *J. Geol. Soc. Lond.*, *155*, 883–891.
- Yin, A., T. M. Harrison (2000), Geologic evolution of the Himalayan-Tibetan Orogen, *Annu. Rev. Earth Planet. Sci.*, *28*, 211–280.
- Zhang, R., M. A. Murphy, T. J. Lapen, V. Sanchez, M. Heizler (2011), Late Eocene crustal thickening followed by Early-Late Oligocene extension along the India-Asia suture zone: Evidence for cyclicity in the Himalayan orogen, *Geosphere*, *7*, 1249–1268, doi: 10.1130/GES00643.1